Ultrasensitive transverse magneto-optical Kerr effect measurements using an effective ellipsometric detection scheme

E. Oblak[1], P. Riego[1,2], A. Garcia-Manso[1], A. Martínez-de-Guerenu[3,4], F. Arizti[3,4], I. Artetxe[3,4], and A. Berger[1]

[1]CIC nanoGUNE, E-20018 Donostia - San Sebastián, Spain

[2]Departamento de Física de la Materia Condensada, Universidad del País Vasco, UPV/EHU, 48080 Bilbao, Spain

[3]CEIT, Manuel Lardizabal 15, 20018 Donostia - San Sebastián, Spain

[4] Tecnun (University of Navarra), Manuel Lardizabal 13, 20018 Donostia - San Sebastián, Spain

Abstract

We present a new methodology that enables a significant sensitivity improvement for transverse magneto-optical Kerr effect (T-MOKE) detection. For this purpose, we developed a novel measurement scheme, in which the polarization detection conditions are changed during the measurement sequence in a pre-defined way. An analytical expression of the associated T-MOKE signal pattern was derived, which allowed us to analyze and classify our experimental data in a straightforward way. Furthermore, this new measurement approach enables the identification of noise and false background signals that might be generated by the sample under investigation, the environment or the detection system itself and it provides a pathway to unambiguously separate all these effects from true T-MOKE signals. These capabilities significantly increase the sensitivity and robustness of T-MOKE detection. The method enabled us to measure magneto-optical signals for samples that are paramagnetic at room temperature or exhibit really small magneto-optical responses, even in the presence of false signals that were far larger in size. Our new methodology was integrated into a scanning wafer tool, which allows for nondestructive, laterally resolved surface characterization measurements and even has the capability of measuring optical and magneto-optical properties simultaneously.

Introduction

The magneto-optical Kerr effect (MOKE) is an important characterization technique and it is a widely applied methodology for the study of magnetism and magnetic materials [1]–[4]. In addition to materials characterization, magneto-optical effects have found a wide range of applications in different scientific and technological fields, including optical isolation [5],[6] magnetoplasmonics [7], ultra-fast magnetization dynamics detection [8]–[10], magnetic switching [11],[12], nanomagnetism [13],[14], spintronics [15]–[17] and bio-sensing [18]–[22], for instance.

The magneto-optical Kerr effect technique relies on small, magnetization induced changes in the optical properties of a material, which in turn modify the polarization or the intensity of reflected light [2]. Conventionally, the Kerr effect is classified according to the magnetization orientation in reference to the sample surface and the plane-of-incidence: When the magnetization is perpendicular to the sample plane, the effect is called polar MOKE, and when the magnetization is in the sample plane, the effect is called longitudinal MOKE or transverse MOKE, with the former referring to the magnetization lying in the plane of incidence, and the latter perpendicular to it [1],[23].

Depending on the specific magnetization orientation, the magnetic material affects different aspects of the reflected light. In the case of polar and longitudinal MOKE, the sample magnetization leads to a rotation and ellipticity change of the reflected light polarization that inverts if the magnetization itself is inverted [24]. In the transverse geometry, one observes in general a change in the intensity of the reflected light for incident p-polarized radiation upon magnetization reversal [25].

In general, T-MOKE tends to produce rather weak signal amplitudes, if compared to longitudinal and especially polar MOKE [24],[26],[27]. The relative change in the reflected light intensity due to the T-MOKE in ferromagnets such as nickel or cobalt is of the order of 10^{-4} to 10^{-3}, limiting T-MOKE applicability [3],[28],[29]. Due to the fact that polarization measurements generally allow for a more sensitive detection, the polar and longitudinal MOKE are more commonly used than the transverse effect and overall preferred by the research community. However, transverse MOKE experiments can be simpler, at least when utilizing traditional measurement set-ups, given that they are mere intensity measurements. Due to this simple operation, they are also particularly suitable for applications [3],[30]. Moreover, the T-MOKE geometry having its optical observation plane oriented perpendicular to the magnetic field allows for a physical separation of optical elements and magnetic field generating components, which makes design and engineering experimental set-ups simpler.

Despite the perceived small signal limit of T-MOKE, it was demonstrated in previous works that with suitable set-up modifications a most significant enhancement of the T-MOKE signal can be achieved. Specifically, these modifications include a mixing of s- and p-polarized light in the incoming beam and the efficient reduction of the detected light amplitude that does not carry magnetic information [29],[31]–[34]. This enhanced T-MOKE signal was also confirmed

in our recent work [35] where we used an effective polarization detection scheme and conducted a detailed and quantitative study of its performance. The study included signal-to-noise ratio measurements and a detailed sensitivity analysis by means of an especially challenging set of samples, in which the magneto-optical signal had been artificially reduced. We reported that by using the effective polarization detection T-MOKE technique, one can achieve very significant improvements with a more than 30-fold increase of the T-MOKE signal and signal-to-noise ratio in comparison to conventional T-MOKE intensity measurements. Our work demonstrated unambiguously that one can reach sensitivities that are normally only associated with longitudinal or polar MOKE measurements.

In the present work, we demonstrate that by means of a novel detection and data analysis scheme, the sensitivity of T-MOKE measurements can be improved even significantly beyond the capabilities of effective polarization detection. For this purpose, we define and analyze a novel measurement scheme, in which the effective polarization detection conditions are changed during the measurement sequence in a pre-defined way. As we will demonstrate, the utilization of such a measurement sequence allows us to extract true magneto-optical signals from experimental data, given that T-MOKE signals will follow a precise and predictable signal pattern, for which we derived an analytical expression. This new measurement approach enables us to identify also noise and false background signals that might be generated by the sample under investigation, the environment or the detection system itself and separate all these effects from true T-MOKE signals. These capabilities significantly increase the sensitivity and robustness of T-MOKE detection, so that our new method achieves unprecedented performance levels.

Furthermore, we adapted our new detection scheme and set-up so that it could be integrated into a scanning wafer tool and thus make spatially resolved and scanning surface measurements viable with our novel method, i.e. allowing measurements of unprecedented sensitivity and robustness across entire surfaces. In order to properly and fully evaluate our new methodology and its sensitivity, we performed a series of measurements on specifically designed samples that are either only weakly ferromagnetic or paramagnetic at room temperature, or exhibit an intentionally reduced magneto-optical response.

Experimental setup

For the implementation of our new T-MOKE methodology, we used the T-MOKE setup geometry that is schematically presented in Fig. 1. In our setup we utilize an ultra low noise laser with a wave length $\lambda = 635$ nm and an angle of incidence of 60° with respect to the surface normal. The laser light first passes through a first linear polarizer P1 and gets subsequently reflected by a sample (not visible in Fig. 1) that is placed inside the gap of an electromagnet. The reflected light beam then passes through a rotatable quarter wave plate QWP and another rotatable linear polarizer P2, after which the net transmitted light intensity is measured with a photo-detector. The incoming polarization axis is set by the P1 polarizer angle θ_1, which we fixed in our experimental study here to 45° with respect to the plane of incidence, given that in

our previous work on the effective polarization T-MOKE method, it resulted in the highest signal levels and signal-to-noise ratios [35].

The described setup is polarization sensitive, in that the light intensity *I* is detected as a function of the applied field *H,* which changes as the magnetization state of the sample changes. In our previous T-MOKE experiments [32], where the orientation of P1, QWP and P2 are fixed, the observed intensity change *ΔI* in between inverted magnetization states is proportional to the T-MOKE induced ellipticity [24],[36]. The fractional intensity change *ΔI/I* upon magnetization reversal (driven by the magnetic field reversal) is defined as:

$$\frac{\Delta I}{I} = 2\frac{I(H)-I(-H)}{I(H)+I(-H)}, \quad (1)$$

where *I* represents the DC-component of the measured intensity and *ΔI* represents the intensity component that is synchronous with the applied magnetic field frequency. *ΔI/I* is a relevant signal that we analyze in our novel T-MOKE methodology.

Fundamentals of ultrasensitive ellipsometric T-MOKE detection

The effective polarization method uses one specific setting for the QWP and P2 orientations (see [35]) to establish a very sensitive configuration, with which one can detect small T-MOKE changes via an effective polarization signal. However, this effective polarization T-MOKE detection method, in spite of having significantly improved sensitivity, does not inherently separate true T-MOKE signals from non-magneto-optical signals that might be caused by the overall experimental conditions of sample or tool. This is especially important when measuring ultra small signals where background noise or false field induced signals (that are not magneto-optical in nature) are superimposed onto much smaller true magneto-optical signals [17]. In order to obtain a greater sensitivity and be able to separate or distinguish true T-MOKE signals from other signals or noise sources we have developed a new approach, the effective ellipsometric T-MOKE detection method. In this ellipsometric method, we perform a sequence of T-MOKE measurements near the effective polarization measurement point, because these experimental conditions were already demonstrated to enable extremely sensitive measurements [33].

The basic idea is hereby that we measure *ΔI/I* signals for different orientations for both elements in the detection arm, i.e. QWP and P2. The obtained signal pattern for different QWP and P2 configurations is caused by the superposition of the magneto-optical T-MOKE response with the purely optically induced ellipticity in reflection, assuming that the incoming light is a mixture of s- and p-polarization. This phase dependent superposition is the key of our new method and by knowing how a real T-MOKE signal is supposed to behave upon changing the orientation of the QWP (i.e. its angle Φ_2) and polarizer P2 (i.e. its angle θ_2), we devised a scheme to interrelate multiple measurements for different detection configurations. Specifically, we derived the mathematical solution for the fractional intensity change *ΔI/I* at

the photo-detector due to magnetization reversal for the true T-MOKE signal that is based upon the material's reflection matrix. This approach employs the same strategy as the generalized magneto-optical ellipsometry (GME) method, which also describes the determination of a reflection matrix by performing *ΔI/I* measurements for a sequential set of polarization detection conditions, and which has been demonstrated to enable a robust separation of optical and magneto-optical signal contributions [37]–[39]. Despite certain similarities related to the interference of optical and magneto-optical polarization effects, the experimental set-up and operation conditions are substantially different for our novel effective ellipsometric T-MOKE method, if compared to the already established GME methodology.

We start the mathematical derivation that describes our experimental set-up, shown in Fig. 1, by considering the total detected light signal *I* at the photo-detector, which is given as

$$I = E_D \cdot E_D{}^* + I_{NM}. \tag{2}$$

Hereby, I_{NM} incorporates any detected light intensity or perceived light intensity due to electrical circuit artifacts that contribute to the total recorded light signal *I*, but are not caused by the ellipsometric reflection from the sample surface and are independent from the QWP and P2 orientation settings. E_D stands for the electric field vector at the photo-detector due to the ellipsometric reflection experiment. Under the assumption that all elements along the optical path conserve the degree of polarization, E_D can be determined via the Jones calculus [40] as

$$E_D = \underline{P2} \cdot \underline{QWP} \cdot \underline{R} \cdot E, \tag{3}$$

where *E* is the electric field vector of the incoming light beam at the sample (i.e. after polarizer P1), *R* is the reflection matrix of the sample, and *P2* and *QWP* are Jones matrices for the linear polarizer and quarter wave plate and are given as

$$\underline{P2} = \begin{bmatrix} cos^2(\theta_2) & \sin(\theta_2)\cos(\theta_2) \\ \sin(\theta_2)\cos(\theta_2) & sin^2(\theta_2) \end{bmatrix} \tag{4}$$

and

$$\underline{QWP} = \begin{bmatrix} cos^2(\Phi_2) + i \cdot sin^2(\Phi_2) & (1 - \mathrm{i})\sin(\Phi_2)\cos(\Phi_2) \\ (1 - \mathrm{i})\sin(\Phi_2)\cos(\Phi_2) & sin^2(\Phi_2) + i \cdot cos^2(\Phi_2) \end{bmatrix}, \tag{5}$$

with θ_2 being the angle between the P2 polarizer axis and the optical plane-of-incidence and Φ_2 as the angle between the QWP axis and the optical plane-of-incidence (see Fig. 1). Because we are only interested in the transverse MOKE here, given our measurement geometry, we can write the reflection matrix *R* for the sample under investigation as

$$\underline{R} = \begin{bmatrix} r_s & 0 \\ 0 & r_p + \beta \end{bmatrix} = r_p \begin{bmatrix} \widetilde{r_s} & 0 \\ 0 & 1 + \tilde{\beta} \end{bmatrix} = r_p \underline{\widetilde{R}}, \tag{6}$$

where r_s and r_p are the conventional complex Fresnel reflection coefficients for s-polarization and p-polarization for a non-magnetic material, respectively, and β is the complex coefficient that represents the transverse magnetization induced contribution to r_p, which switches its sign upon magnetization reversal.

Given the above, we calculated the mathematical solution for the fractional intensity change at the photo-detector *ΔI/I* (with Eq. (1) and Eq. (2)) due to magnetization reversal for any combination of the optical element orientations, including any arbitrary incoming polarization angle θ_1 (with θ_1 being the angular distance between the first polarizer axis and the plane-of-incidence). As already indicated in Eq. (2), we also take into account the detected intensity signal I_{NM} that occurs, but is not related to the ellipsometric optical and magneto-optical effects of the sample. Specifically, we find that

$$\frac{\Delta I}{I} = 4\frac{B_1 \sin^2\theta_1\, h_2 + \cos\theta_1 \sin\theta_1[(B_1B_3+B_2B_4)h_3-(B_1B_4-B_2B_3)h_4]+\frac{1}{2}B_6}{(B_3^2+B_4^2)\cos^2\theta_1\, h_1+\sin^2\theta_1\, h_2+2\cos\theta_1 \sin\theta_1(B_3h_3-B_4h_4)+\frac{1}{2}B_5} \tag{7}$$

with

$$\begin{aligned} h_1 &= \frac{\cos^2(2\Phi_2-\theta_2)}{2}+\frac{\cos^2(\theta_2)}{2} \\ h_2 &= \frac{\sin^2(2\Phi_2-\theta_2)}{2}+\frac{\sin^2(\theta_2)}{2} \\ h_3 &= \frac{\sin(4\Phi_2-2\theta_2)}{4}+\frac{\sin(2\theta_2)}{4} \\ h_4 &= \frac{\sin(2\Phi_2-2\theta_2)}{2} \end{aligned} \tag{8}$$

and

$$\begin{aligned} B_1 &= Re(\tilde{\beta}) \\ B_2 &= Im(\tilde{\beta}) \\ B_3 &= Re(\tilde{r}_s) \\ B_4 &= Im(\tilde{r}_s) \end{aligned} \tag{9}$$

For the specific case that we implemented experimentally, namely θ_1= 45°, Eq. (7) simplifies to:

$$\frac{\Delta I}{I} = 4\frac{B_1\cdot h_2 + (B_1B_3+B_2B_4)\cdot h_3 - (B_1B_4-B_2B_3)\cdot h_4 + B_6}{(B_3{}^2+B_4{}^2)\cdot h_1 + h_2 + 2\cdot B_3\cdot h_3 - 2\cdot B_4\cdot h_4 + B_5}, \tag{10}$$

The derived intensity change equations, Eq. (7) and Eq. (10), are primarily defined by products of the elements of the reflection matrix, i.e. B_1 – B_4, where B_1 and B_2 present the real and

imaginary part of the magneto-optical parameter $\tilde{\beta}$, and B_3 and B_4 present the real and imaginary part of the optical parameter $\tilde{r}_s$. The described fitting parameters B_1 – B_4 are multiplied by trigonometric functions that contain the orientation angles of the optical elements of the experiment. These parts describe the ellipsometric effects under the assumption of a perfect experimental system. In addition, Eqs. (7) and (10) include two corrective terms that correspond to I_{NM} and are both independent from QWP and P2 orientation settings. B_5 describes the fact that even for the QWP and P2 orientation settings that minimize I and even if there is no modulation of magnetic field frequency, the transmitted light intensity is not zero due to imperfections of the optical elements, but instead has a non-vanishing value, which is B_5.

B_6 describes the fact that there might be a non-T-MOKE $\Delta I/I$ signal, which enters the detection circuit either optically or electrically. Given that in any specific experimental implementation, ΔI is triggered via a certain magnetic field change procedure, i.e. via a certain field modulation, ΔI represents the intensity component that is synchronous with the applied field frequency and B_6 represents the non-T-MOKE signal part of I_{NM} that has the same frequency as the field modulation, and thus as the T-MOKE ΔI signal. It is exactly this component of I that can lead to misinterpreted results, because it follows the correct modulation frequency, but does not have a magneto-optical origin and cannot be discriminated in a conventional MOKE experiment. This false signal, however, can now be separated out, because it does not have the same (Φ_2, θ_2) dependence as the true T-MOKE signal. For the present study, we simply assume the false ΔI signal to be independent from Φ_2 and θ_2, and being represented by its amplitude B_6. More sophisticated false signal models could be derived and are compatible with our ellipsometric T-MOKE detection method, but turned out not to be necessary in our experimental tests.

With our novel ellipsometric methodology, we have now devised a measurement scheme that can be very sensitive by operating near the (Φ_2, θ_2) light compensation point, as well as being highly discriminative, because true magneto-optical signals will have a clearly identifiable signature. The derived solutions, Eqs. (7) and (10), describe an exact signal pattern that is produced upon varying QWP and P2 orientation angles (Φ_2 , θ_2). In its practical implementation here, the data are recorded as $\Delta I/I$ measurements for a grid of preselected (Φ_2, θ_2) values. The data analysis is subsequently accomplished by fitting all experimental data against the predicted T-MOKE signal pattern as a function of Φ_2 and θ_2 using Eq. (10), given that we specifically choose $\theta_1 = 45°$. As a result we obtain the magneto-optical behavior as a function of preselected (Φ_2, θ_2) values and with determination of fitting parameters B_1-B_4 we are able to determine the reflection matrix parameters $\tilde{r}_s$ and $\tilde{\beta}$, which represent the optical ($\tilde{r}_s$) and magneto-optical ($\tilde{\beta}$) properties of the measured sample. Upon determining the complex reflection coefficients $\tilde{r}_s$ and $\tilde{\beta}$ we can in turn determine the complex dielectric constant or index of refraction for any bulk material. The preselection of the angle range (Φ_2, θ_2) and its dependence on the sensitivity of the measurements is very much sample dependent. Samples with very low reflectivity will generally require larger (Φ_2, θ_2) ranges, simply because otherwise the total light intensity and thus light induced voltages at the photo-detector are too small to be optimally detected.

The general and practical viability of our novel method is demonstrated in Fig. 2, where we present in Fig. 2(a) an example of $\Delta I/I$ data recorded for a $Co_{0.76}Ru_{0.24}$ sample as a function of Φ_2 and θ_2 in a color-coded map. Despite having a rather low magnetization and Curie temperature (T_C = 460 ± 10 K) [41], the sample produces a strong T-MOKE signal due to the fact that we operate near the optimized effective polarization measurement point. In addition, we observe a zero crossing point and an asymmetric structure of the signal pattern, consistent with the mathematical expression of Eq. (10). When we compare this experimental result to our theoretical T-MOKE prediction (Fig. 2(b)) according to Eq. (10), we can see that the measured data in Fig. 2(a) are in almost perfect agreement with the least-squares fit (Fig. 2(b)) that we obtained by utilizing Eq. (10) as the fit function and the 4 B_i as fit parameters. This indicates that our methodology allows for a very precise quantitative determination and analysis of the true magneto-optical behavior using T-MOKE. In addition, the optical properties of the sample are determined simultaneously via the fit parameters B_3 and B_4.

For the specific data shown in Fig. 2(a), we apply signal detection and filtering procedures of the photo-detector signal, whose operation is illustrated in Fig. 3. In Fig. 3(a) we present the AC magnetic field, which is generated via an AC current that drives the electromagnet of our set-up. The synchronously detected light signal at the photo-detector follows the applied magnetic field and changes as the magnetization state of the sample inverts, such as can be seen in Figs. 3(b) and (c). Fig. 3(b) presents the detected light intensity for a ferromagnetic sample exhibiting a nearly square-wave signal, while Fig. 3(c) shows an example for the light signal trace that is generated by a non-ferromagnetic sample, resulting in a very small and thus noisy signal. The mean value of the measured photo-detector intensity denotes our intensity I value as indicated in the figure. The blue solid lines in Figs. 3(b) and (c) represent the filtered and reconstructed signals from the amplitudes of the Fourier series after a FFT analysis of the measured intensity signal. Since we want to be able to describe the square wave like response one finds for a ferromagnetic material (see Fig. 3(b)), we take into consideration the odd components of the first seven amplitudes of the Fourier series extracted from the I vs. time signal trace. Higher order contributions do not turn out to be significant. The corresponding net ΔI signal amplitude we can then calculate from these amplitudes of the Fourier series as $\Delta I = 2(A_1-A_3+A_5-A_7)$ with A_i being the i-th order amplitude of the Fourier series. Here, we defined all A_i as positive number, so that the 3_{rd} and 7_{th} order contribute negatively to the center wave intensity change due to their inverted phases.

In order to test and apply our novel methodology and perform measurements on relevant samples, we assembled a new experimental setup that allows for an automated operation of our ellipsometric T-MOKE detection scheme at pre-selected sample spots on a surface. The tool that we designed and built is presented in Fig. 4. Specifically, Fig. 4(a) presents a schematic design of the tool and Fig. 4(b) shows a photo of the actual tool that was used for our experiments. The detection head of the tool, which is the entire upper portion of our tool in Fig. 4, consists of an illumination arm, a magnet and a detection arm. On the illumination arm, we have a laser source mounted onto a holder that allows for corrections in XY direction and tilt, as well the first polarizer P1 that can be rotated manually to select the desired polarization for

the incoming light beam. The magnet is fixed on a linear stage in order to be able to adjust the distance in between the sample and magnet. The sample itself is not connected to the detection head assembly but lies on a separate sample holder below. On the detection arm, we have a QWP followed by the second polarizer P2, of which both are mounted inside motorized rotation stages, which allows us to change the QWP and P2 orientations Φ_2 and θ_2 automatically during measurements with a resolution of $2 \cdot 10^{-4}$ deg. The last element on a detection arm is a photo-detector mounted on a XY-translation stage that allows for the alignment of the sample reflected laser spot onto the center of the photo-detector diode. Below the detection head, we placed a sample holder assembly mounted on a XY-scanning table, which enables wafer scan measurements over any preselected scan area. Furthermore, all key components of the setup are assembled in such a way that optimized alignment in between the various parts is easily achieved, and furthermore vibrations and electrical interference in between the elements are avoided.

For the entirety of the measurement and data analysis sequence, we have furthermore developed a control software that enables easy operation, such as: control of the scanning table system, including sample loading and unloading, as well as preselecting the area of interest; selecting the frequency and amplitude of the magnetic field, driven by a home-made AC-drive current system and controlled by a Hall probe sensor; automatically finding a suitable ellipsometric operation point and/or range; measurement execution for preselected angle pairs, including data acquisition and filtering of the photo-detector signal, as well as ellipsometric T-MOKE data analysis according to Eqs. (7) or (10).

Experimental Results

The capabilities of our method and suitability of our actual tool are demonstrated in the following, where we present results obtained on several samples, which include specific materials with extremely small magnetic and magneto-optical effects. For this purpose, we designed a series of samples, in which we alloyed Co with Ru, and thus create alloys that are either only weakly ferromagnetic at room temperature, or are paramagnetic at room temperature, but with a still detectable paramagnetic response. We fabricated these samples as thin films via sputter deposition, using Si wafers as substrates, on which a 50 nm layer of each specific CoRu layer was deposited and which was subsequently coated with 10 nm of SiO_2 to avoid surface oxidation. In addition, we performed structural and conventional magnetic characterization measurements and then utilized these samples to explore the capabilities of our novel methodology and tool. In Fig. 5 we present exemplary results of conventional magnetometry for two of these samples. As one can clearly see, the 24% Ru containing sample ($Co_{0.76}Ru_{0.24}$) exhibits a still robust ferromagnetic signal at room temperature and thus, it is not surprising that is shows a significant T-MOKE effect. We have therefore utilized its results already in Fig. 2(a) to demonstrate the fundamental operation of our novel method. Given that the data showed a nearly perfect match to the anticipated ellipsometric T-MOKE signal, including the expected signal symmetry, no additional discussion of these results are needed. Instead, we focus here on the 32% Ru containing sample ($Co_{0.68}Ru_{0.32}$), which, as we can see

in Fig. 5, exhibits no visible ferromagnetism at room temperature, and thus is a far more challenging test object for our methodology.

In contrast to the rather simple T-MOKE signal case of Fig. 2, the *ΔI/I* signal for the non-ferromagnetic $Co_{0.68}Ru_{0.32}$ sample in Fig. 6(a) does not visibly display the expected magneto-optical response pattern and its asymmetric key feature. Also, the data reveal that the overall signal level is vastly reduced if compared to that of the data in Fig. 2. Upon closer inspection, one notices that the main feature of the data pattern in Fig. 6(a) resembles the inverse of the total light intensity that is produced by the respective optical element settings. This in turn means that the main contribution to the signal measured by the photo-detector circuit is not magneto-optical in nature and is actually not impacted by the specific QWP and P2 orientation settings. Instead, it is a constant false signal that is synchronous with the applied field frequency, but independent from the T-MOKE effect.

The existence of this false signal now permits us to demonstrate the remarkable potential of our methodology, because our analysis scheme according to Eq. (10) allows the method to cope with such false signals in the form of fit parameter B_6. As we will see, this even works if the false signals are much larger than the actual T-MOKE signal, because their characteristic Φ_2 and θ_2 dependence is completely different to that of a true T-MOKE signal. This can now be seen in Figs. 6(b) – (d). Fig. 6(b) shows the actual data fit according to Eq. (10) to the data shown in Fig. 6(a) and it is obvious that even these false signal dominated data can be described with an extremely high level of accuracy, achieving an R_2 value of 0.989. The fact that a true T-MOKE signal is actually present in this sample and can be extracted by means of our method, is visualized in Figs. 6(c) and (d), where we show the data and the fit, respectively, after removing of the false signal contribution to the data. Both clearly show the typical sign-inversion pattern of a true T-MOKE effect and they match each other very well, even if the actual T-MOKE signal is about one order of magnitude smaller than the false signal that is superimposed onto it. These results demonstrate the sensitivity and ability of the methodology to measure magneto-optical properties even for non-ferromagnetic samples with extremely low magneto-optical signals, as well as in the presence of synchronous false signals. Also, from fitting parameters B_1 and B_2 we can extract real and imaginary values of magneto-optical parameter $\tilde{\beta}$ that are listed in Table I. The values in Table I show that with this method we are able to achieve effective signal-to-noise-ratios of about 50 even if the signal is of the order of only several 10^{-6}.

These abilities of our novel methodology are corroborated by measurements on another sample that again exhibits a very small magneto-optical signal. This sample was selected from a specifically designed series of coated cobalt films, for which the T-MOKE signal is artificially reduced by means of a Ag overcoat [35]. Here we present results for a cobalt sample with 80 nm Ag overcoat, for which 99.8% of the reflected light actually come from the Ag layer and therefore do not carry a magneto-optical signal, making this sample another most challenging test case. In Fig. 7(a) we present the measured *ΔI/I* signal pattern again as a color-coded map, and similar to the data in Fig. 6, the pattern does not visibly display the magneto-

optical response features. Instead, the main feature of the data pattern resembles again the inverse of the total light intensity at every respective setting. Thus, also here the main contribution to the signal measured by the photo-detector is a false signal that is synchronous with the applied field frequency, but independent from the T-MOKE effect. The fit of the data according to Eq. (10) is presented in Fig. 7(b) with a goodness value of $R_2 = 0.986$. Just as in the previous example of Fig. 6, we are still able to extract the relatively weak actual T-MOKE signal by means of our ellipsometric method. The true T-MOKE signal is visible in Figs. 7(c) and (d), where we show the data and the fit, respectively, after removal of the false signal. The so-extracted data pattern show the typical sign-inversion of a true T-MOKE effect and the numerical values of the magneto-optical fit parameters B_1 and B_2, listed in Table I, demonstrate that this method can achieve effective signal-to-noise-ratios of about 100, even for signals of the order of several 10^{-6}, from which we estimate sensitivity levels of several 10^{-8} for our tool. Moreover, with this example we want to emphasize the improved sensitivity of our new methodology, with which we achieved more than a 7-fold increase of the effective signal-to-noise-ratio in comparison with the results reported in [35] where we measured the T-MOKE signal of the same sample but via the effective polarization detection measurement scheme.

The potential of our experimental tool and its integrated ellipsometic T-MOKE methodology to perform nondestructive laterally resolved surface characterization measurements is presented in Fig. 8 in an exemplary fashion. Fig. 8 presents an example of wafer scan measurements over a 40 mm x 40 mm section of a 100 mm diameter paramagnetic $Co_{0.68}Ru_{0.32}$ wafer sample that we fabricated with the intent of making a uniform film[1]. The same sample was scanned in two different orientations, i.e. orientation O1 (Fig. 8 - first row) and orientation O2 (Fig. 8 - second row), for which the sample was rotated by 90° with respect to O1. The color-coded maps here show the local magneto-optical Fig. 8(a, b, c, e, f, g) and optical (Fig. 8(d, h)) response as a function of sample position. From the maps in Fig. 8 one can see that there is a gradual and not insignificant change of parameter $\tilde{\beta}$ over the scanned sample surface (Fig. 8(a, b, e, f)). Specifically, the absolute values of parameter $\tilde{\beta}$, shown in Figs. 8(c) and (g), indicate that there is a gradient-like 140% variation (if referenced to the map average) of the local magneto-optical response across the scan area. The comparison of Fig. 8(c) and Fig. 8(g) furthermore shows that the direction of the gradient rotates by 90° when we rotate the sample by 90°, confirming that our observations is an actual sample feature and not related to possible experimental drift. At the same time, we can see that the optical properties of the sample presented in Figs. 8(d) and (h) do not exhibit any obvious change in the entire scanned area, even though the color-scale for the optical measurements is limited to ±10% only. These results show the potential of our methodology due to its ability of measuring optical and magneto-optical responses simultaneously and by doing so identify surface non-uniformities that can't be detected by using conventional ellipsometric measurements that only analyze optical properties. Lastly, it should be noted that we have achieved this demonstration for a paramagnetic material, which exhibits an extremely weak magneto-optical response only.

[1] The $Co_{0.68}Ru_{0.32}$ sample was fabricated by co-sputtering from two sputter guns to mix Co and Ru at the intended stoichiometry while aligning the guns towards the substrate, which was rotated during deposition with the goal of achieving uniformity all across the 100 mm diameter wafer.

Nonetheless, we could detect it robustly and repeatedly, as demonstrated by the entirety of the scans shown in Figs 8(c) and (g).

Discussion and conclusions

In this study we have presented a new methodology that allows for a significant improvement of the sensitivity for T-MOKE detection systems. The improved sensitivity is especially important if one wants to measure samples with small magneto-optical signals that are otherwise undetectable due to the presence of non-magneto-optical false signals that can occur in any experimental system.

We have shown that with an appropriate detection system and scheme based on an ellipsometric measurement and data evaluation approach, we are capable of reliably identifying and extracting even extremely small magneto-optical signals. In our experimental system, we performed such ellipsometric T-MOKE detection measurements by varying the QWP and P2 orientations and by utilizing an incoming light polarization that is a mixture of s- and p-polarized light. The functionality of the method is hereby achieved via the varying superposition of the magneto-optical T-MOKE response with purely optically induced ellipticity in reflection. Given that such a phase dependent superposition of polarized light is generally the basis for ellipsometry, we are referring to our new approach as an ellipsometric measurement scheme here. However, it is also worthwhile noting that we operate only near light extinction conditions, because in this regime T-MOKE leads to large $\Delta I/I$ values, which also adds to the achieved sensitivity of our method.

We derived a mathematical description of how a real T-MOKE signal behaves upon changing the orientation of the QWP (i.e. its angle Φ_2) and polarizer P2 (i.e. its angle θ_2) in our setup. The accuracy of the derived solution was demonstrated by experiments on a $Co_{0.76}Ru_{0.24}$ sample, which has a relatively strong T-MOKE signal, and thus clearly displayed the predicted signal pattern. However, our analysis of the signal generated in our experimental setup also considered the fact that optical and electrical imperfections are present and that the T-MOKE signal producing field excitation can also produce false signals that are unrelated to T-MOKE. These false signals are taken into account and a total detected light intensity is defined as a sum of the true ellipsometric signal that depends on the QWP and P2 position angles and false signal components that are also present in the detection channel, but do not exhibit the proper MOKE signal pattern. We are therefore able to separate out the light signal portions that are not related to T-MOKE, because they do not have the same angle (Φ_2, θ_2) dependencies that a true T-MOKE signal exhibits. This real-from-false signal separation allows us to detect extremely small magneto-optical signals that are otherwise hidden underneath a much bigger false signal, which is simultaneously present in the detection system. This was demonstrated for a paramagnetic $Co_{0.68}Ru_{0.32}$ sample, for which the main contribution to the signal measured in the detector was not magneto-optical in nature. Nonetheless, we were able to extract the true T-MOKE signal even if it was one order of magnitude smaller than the superimposed false signal. So, in essence our methodology represents a very efficient filtering scheme that allows

for ultrasensitive T-MOKE-signal detection and recovery. The fitting parameters of the mathematical solution for detected *ΔI/I* signals allow us to obtain the magneto-optical ($\tilde{\beta}$) and optical parameters ($\tilde{r}_s$) of the detected surfaces and it was demonstrated that for our tool we have achieved a detection sensitivity level of the order of several 10^{-8}.

Furthermore, we demonstrated that our new experimental setup allows for ultrasensitive ellipsometric T-MOKE measurements of entire surface areas and permits nondestructive laterally resolved surface characterization measurements. This was shown via scanning experiments on a $Co_{0.68}Ru_{0.32}$ sample, which has a very small magneto-optical response. Hereby, we have demonstrated that our tool allows for a scanning characterization of sample uniformity (or non-uniformity) with excellent absolute and relative precision. Moreover, the fact that our methodology detects optical and magneto-optical properties simultaneously, provides our tool with the ability to identify surface non-uniformities that cannot be detected by conventional ellipsometry alone.

Acknowledgment

We acknowledge support from the Basque Government under the Elkartek program, project No. KK 2016/00025. Work at CIC nanoGUNE was supported by the Spanish Ministry of Economy, Industry and Competitiveness under the Maria de Maeztu Units of Excellence Programme (MDM-2016-0618) and Project No. FIS2015-64519-R (MINECO/FEDER). P.R. acknowledges “la Caixa” Foundation for her Ph.D. fellowship.

Figures

Fig. 1: Experimental setup for T-MOKE detection consisting of laser source, first polarizer (P1), quarter wave plate (QWP), second polarizer (P2) and photo-detector. The polarization angle θ_1 for P1, the orientation angle Φ_2 for QWP and the polarization angle θ_2 for P2 are all defined in the figure and their numerical values are given as the angular distance between each optical element's axis and the optical plane-of-incidence. The sample under investigation (not visible) is located inside the gap of an electromagnet that produces a magnetic field transverse to the plane-of-incidence. The path of the laser light is indicated in the figure.

Fig. 2: Color-coded maps, representing (a) the measured $\Delta I/I$ signal as a function of QWP angle Φ_2 and P2 angle θ_2 for a $Co_{0.76}Ru_{0.24}$ sample, and (b) the corresponding theoretical $\Delta I/I$ signal according to Eq. (10). The colour codes are identified on the right-hand side of each image. The measurements were obtained with an applied magnetic field strength of 300 Oe.

Fig. 3: (a) AC magnetic field vs. time generated with our experimental control system; (b) photo-detector voltage signal vs. time measured on a cobalt sample with 40 nm Ag overcoat. (c) Photo-detector voltage signal vs. time measured on a non-ferromagnetic $Co_{0.68}Ru_{0.32}$ sample. For both samples the intensity I is obtained as the mean value of the detected photo-detector voltage. ΔI is calculated from the amplitudes of the Fourier series as $\Delta I = 2(A_1 - A_3 + A_5 - A_7)$, where A_i represents i_{th} order of the Fourier series. The filtered and reconstructed signals, based upon A_1 *to* A_7 are shown as blue solid lines, while the grey curves represent the unfiltered detector signals in (b) and (c).

Fig. 4: (a) Schematic of the experimental setup used for effective ellipsometry T-MOKE measurements. The detection tool consist of the detection head (upper part), sample holder and scanning table. (b) Photo of the constructed detection tool with detection head, sample holder and scanning table, which was used for all the measurements in this work.

Fig. 5: Magnetization M vs. applied field H measurements for a 24% Ru-alloy sample ($Co_{0.76}Ru_{0.24}$) and a 32% Ru-alloy sample ($Co_{0.68}Ru_{0.32}$).

Fig. 6: Color-coded maps, representing: (a) The measured $\Delta I/I$ signal as a function of QWP angle Φ_2 and P2 angle θ_2 for a non-ferromagnetic $Co_{0.68}Ru_{0.32}$ sample, and (b) the corresponding fit of the measured $\Delta I/I$ signal according to Eq. (10); (c) The extracted magneto-optical $\Delta I/I$ signal (experimental data after removing the false signal contribution to the data) as a function of QWP angle Φ_2 and P2 angle θ_2, for a non-ferromagnetic $Co_{0.68}Ru_{0.32}$ sample, and (d) the corresponding fit of the extracted magneto-optical $\Delta I/I$ signal. The colour codes are identified on the right-hand side of the image.

Fig. 7: Color-coded maps, representing: (a) The measured $\Delta I/I$ signal as a function of QWP angle Φ_2 and P2 angle θ_2 for a cobalt sample with 80 nm Ag overcoat, and (b) the corresponding fit of the measured $\Delta I/I$ signal according to Eq. (10); (c) The extracted magneto-

optical *ΔI/I* signal (experimental data after removing the false signal contribution to the data) as a function of QWP angle Φ_2 and P2 angle θ_2, for a cobalt sample with 80 nm Ag overcoat, and (d) the corresponding fit of the extracted magneto-optical *ΔI/I* signal. The colour codes are identified on the right-hand side of the image.

Fig. 8: Color-coded wafer images of a 40 mm x 40 mm scan area for a 100 mm diameter wafer coated with a paramagnetic $Co_{0.68}Ru_{0.32}$ film sample, measured by utilizing our effective ellipsometric T-MOKE system; the upper and lower row, (a)-(d) and (e)-(h) respectively, represent the same measured quantities for the sample being scanned in two different orientations. In between those two measurements, the sample was rotated by 90°. The scans show different reflection matrix parameters, specifically $Re(\tilde{\beta})$ (a, e), $Im(\tilde{\beta})$ (b, f), $|\tilde{\beta}|$ (c, g), and $|\tilde{r}_s|$ (d, h). For the better visibility of lateral property changes, (c, d, g, h) are shown in a suitable percentage scale, for which 100% represents the area-averaged signal in each case: (c) $1.09 \cdot 10^{-5} = 100\%$, (g) $1.19 \cdot 10^{-5} = 100\%$, (d) $1.068 = 100\%$, (h) $1.046 = 100\%$. For each sub-figure, the respective color scale is displayed on its right side.

Fig. 1

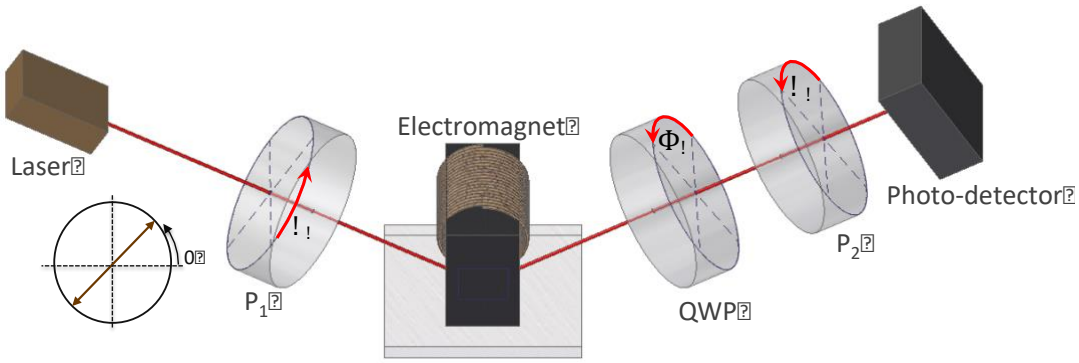

Fig. 2

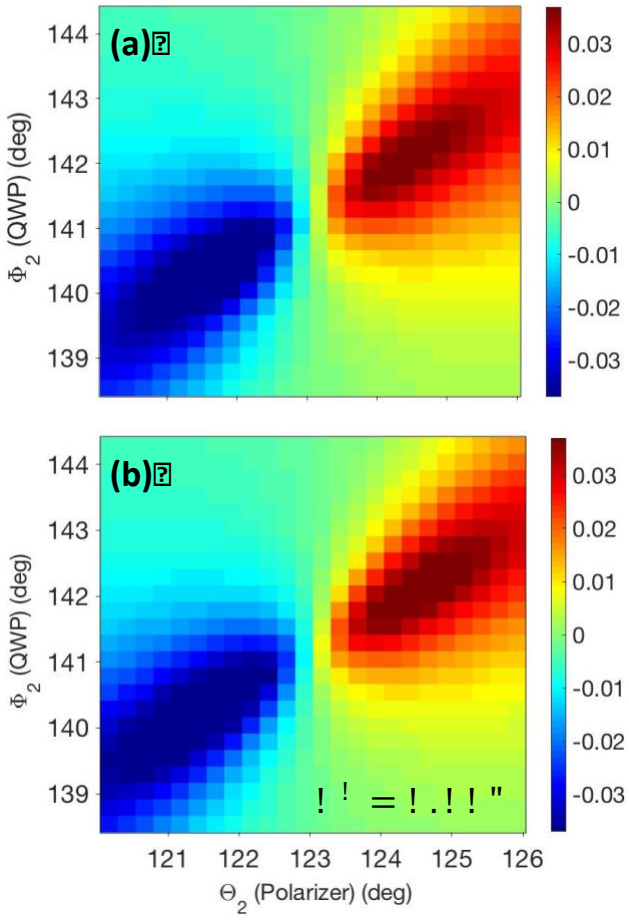
(a)
(b)
144
143
142
141
140
139
Φ2 (QWP) (deg)
0.03
0.02
0.01
0
-0.01
-0.02
-0.03
121
122
123
124
125
126
Θ2 (Polarizer) (deg)

Fig. 3

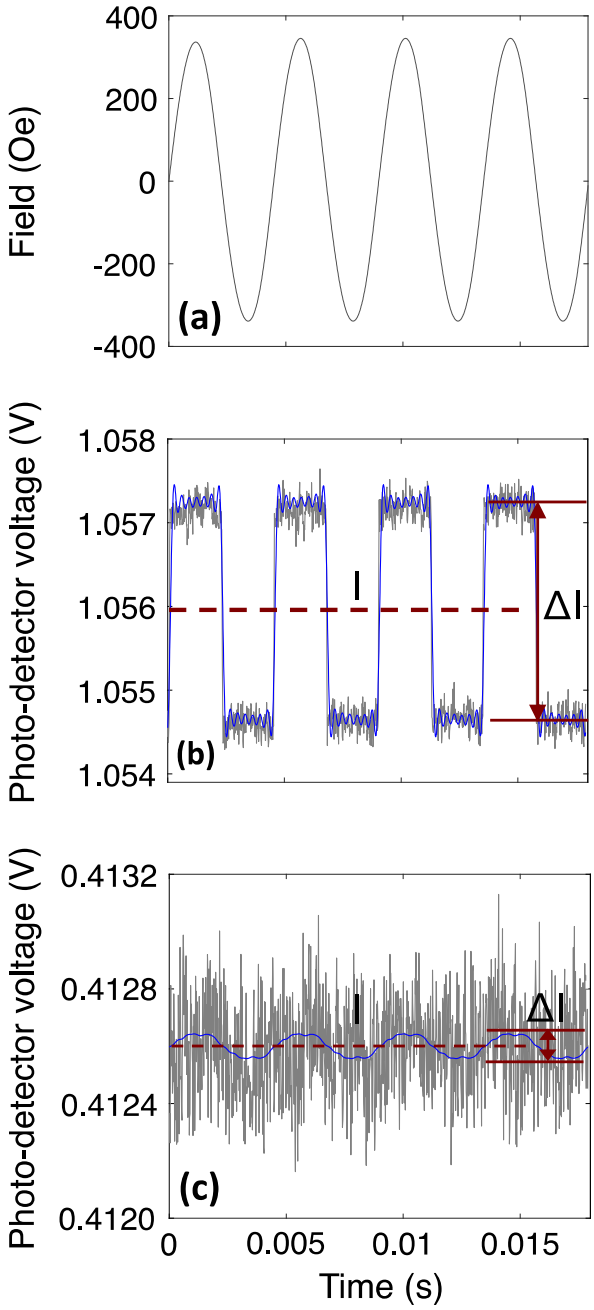
400
200
0
-200
-400
Field (Oe)
(a)
1.058
1.057
1.056
1.055
1.054
Photo-detector voltage (V)
I
ΔI
(b)
0.4132
0.4128
0.4124
0.4120
Photo-detector voltage (V)
I
ΔI
(c)
0
0.005
0.01
0.015
Time (s)

Fig. 4

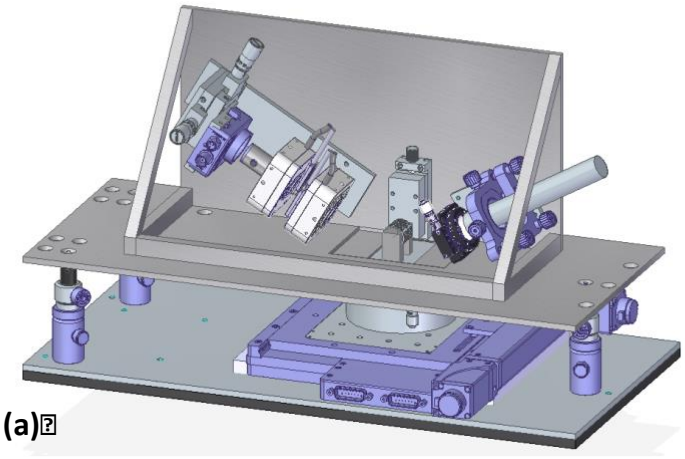

(a)

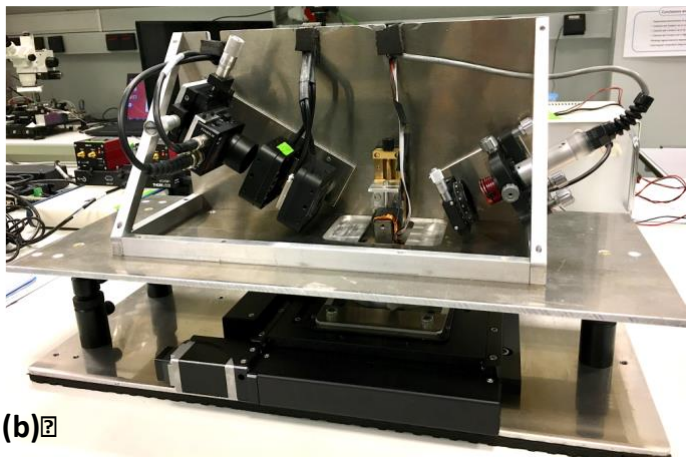

(b)

Fig. 5

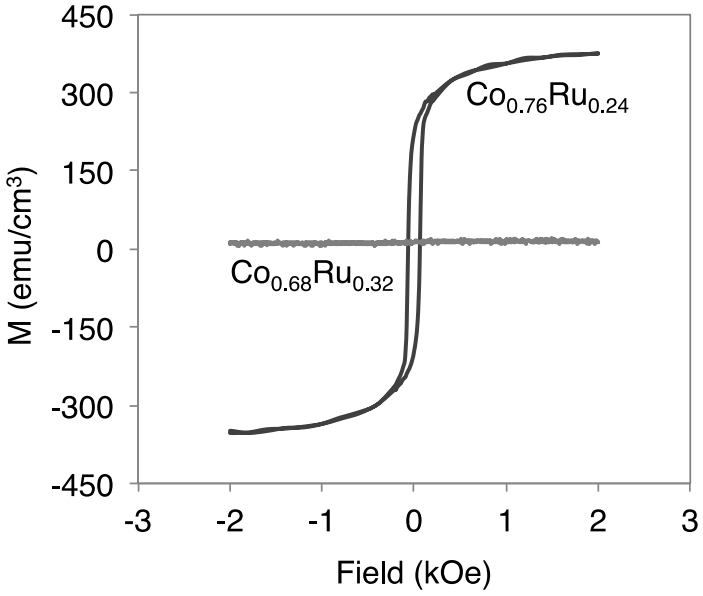
450
300
150
0
-150
-300
-450
M (emu/cm3)
-3
-2
-1
0
1
2
3
Field (kOe)
Co0.76Ru0.24
Co0.68Ru0.32

Fig. 6

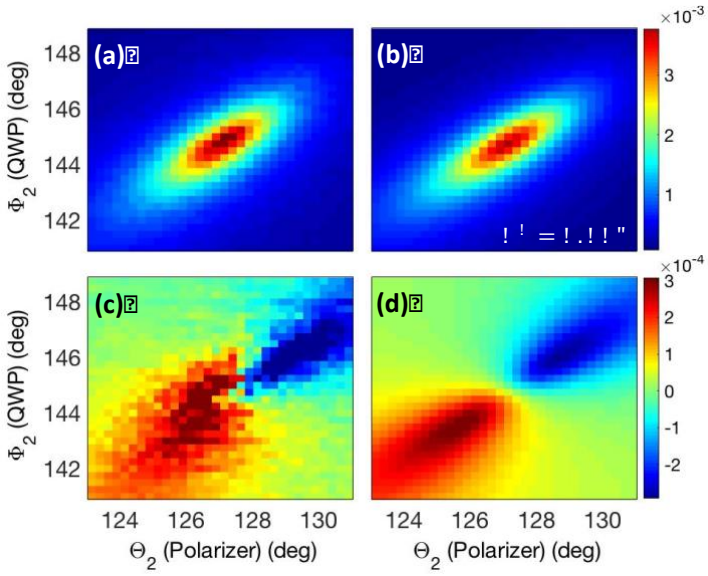
(a)
(b)
(c)
(d)
148
146
144
142
Φ2 (QWP) (deg)
×10-3
3
2
1
×10-4
3
2
1
0
-1
-2
124
126
128
130
Θ2 (Polarizer) (deg)

Fig. 7

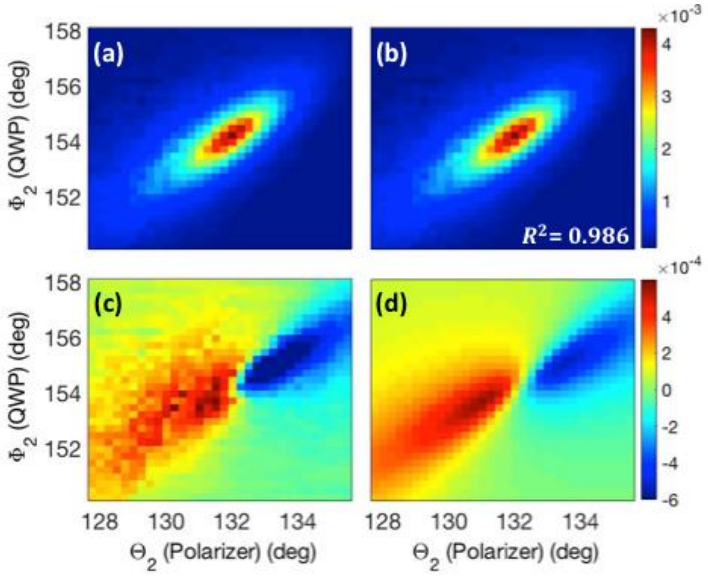
(a)
(b)
(c)
(d)
R^2= 0.986
Φ_2 (QWP) (deg)
158
156
154
152
Θ_2 (Polarizer) (deg)
128
130
132
134
×10^-3
4
3
2
1
×10^-4
4
2
0
-2
-4
-6

Fig. 8

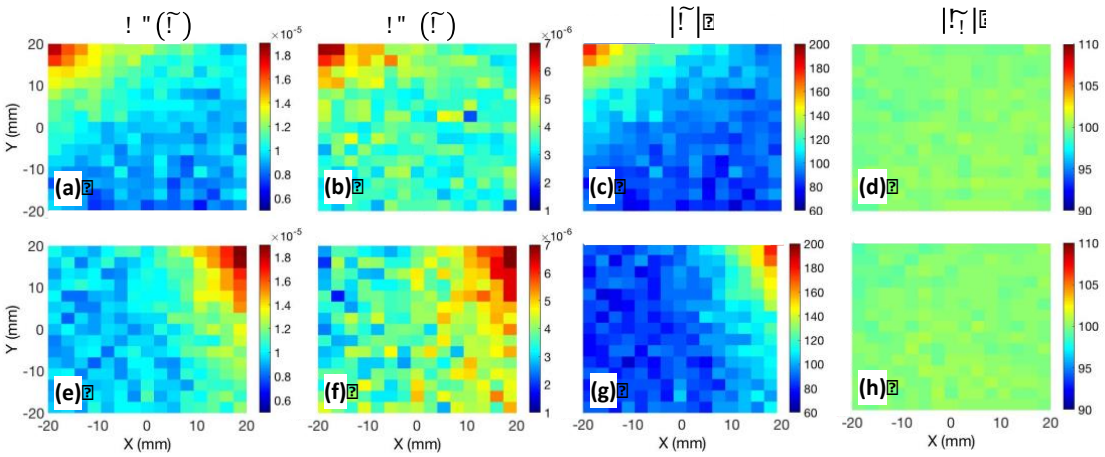

Table I

$Co_{0.68}Ru_{0.32}$	
$\boldsymbol{Re}(\widetilde{\boldsymbol{\beta}})$	$5.67 \cdot 10^{-6} \pm 1.09 \cdot 10^{-7}$
$\boldsymbol{Im}(\widetilde{\boldsymbol{\beta}})$	$4.58 \cdot 10^{-7} \pm 7.99 \cdot 10^{-8}$
Co-film covered by 80 nm Ag	
$\boldsymbol{Re}(\widetilde{\boldsymbol{\beta}})$	$7.52 \cdot 10^{-6} \pm 7.54 \cdot 10^{-8}$
$\boldsymbol{Im}(\widetilde{\boldsymbol{\beta}})$	$2.56 \cdot 10^{-6} \pm 5.65 \cdot 10^{-8}$

References

[1] Freiser, M. A survey of magnetooptic effects. *IEEE Transactions on Magnetics* 4**,** 152–161 (1968).

[2] Qiu, Z. Q. and Bader, S. D. Surface magneto-optic Kerr effect (SMOKE). *J. Magn. Magn. Mater.* 200**,** 664–678 (1999).

[3] Zvezdin, A. K. and Kotov, V. A. *Modern magnetooptics and magnetooptical materials*. (CRC Press, 1997).

[4] Sander, D. *et al.* The 2017 Magnetism Roadmap. *J. Phys. D. Appl. Phys.* 50**,** 363001 (2017).

[5] Gauthier, D. J., Narum, P. and Boyd, R. W. Simple, compact, high-performance permanent-magnet Faraday isolator. *Opt. Lett.* 11**,** 623–625 (1986).

[6] Zamani, M., Ghanaatshoar, M. and Alisafaee, H. Adjustable magneto-optical isolators with high transmittance and large Faraday rotation. *J. Opt. Soc. Am. B* 28**,** 2637–2642 (2011).

[7] Temnov, V. V *et al.* Active magneto-plasmonics in hybrid metal–ferromagnet structures. *Nat. Photonics* 4**,** 107 (2010).

[8] Beaurepaire, E., Merle, J.-C., Daunois, A. and Bigot, J.-Y. Ultrafast Spin Dynamics in Ferromagnetic Nickel. *Phys. Rev. Lett.* 76**,** 4250–4253 (1996).

[9] Cinchetti, M. *et al.* Spin-Flip Processes and Ultrafast Magnetization Dynamics in Co: Unifying the Microscopic and Macroscopic View of Femtosecond Magnetism. *Phys. Rev. Lett.* 97**,** 177201 (2006).

[10] Razdolski, I. *et al.* Analysis of the time-resolved magneto-optical Kerr effect for ultrafast magnetization dynamics in ferromagnetic thin films. *J. Phys. Condens. Matter* 29**,** 174002 (2017).

[11] Stanciu, C. D. *et al.* All-optical magnetic recording with circularly polarized light. *Phys. Rev. Lett.* 99**,** 1–4 (2007).

[12] Lambert, C.-H. *et al.* All-optical control of ferromagnetic thin films and nanostructures. *Science (80-.).* 345**,** 1337–1340 (2014).

[13] Review, T., Grimsditch, M. and Vavassori, P. The diffracted magneto-optic Kerr effect : what does it tell you ? 16**,** 275–294 (2004).

[14] Verduci, T. *et al.* Fourier magnetic imaging. *Appl. Phys. Lett.* 99**,** 92501 (2011).

[15] Puebla, J. *et al.* Direct optical observation of spin accumulation at nonmagnetic metal/oxide interface. *Appl. Phys. Lett.* 111**,** 092402 (2017).

[16] Stamm, C. *et al.* Magneto-Optical Detection of the Spin Hall Effect in Pt and W Thin Films. *Phys. Rev. Lett.* 119**,** 87203 (2017).

[17] Riego, P. *et al.* Absence of detectable current-induced magneto-optical Kerr effects in Pt, Ta, and W. *Appl. Phys. Lett.* 109**,** (2016).

[18] Regatos, D., Sepúlveda, B., Fariña, D., Carrascosa, L. G. and Lechuga, L. M. Suitable combination of noble/ferromagnetic metal multilayers for enhanced magneto-plasmonic biosensing. *Opt. Express* 19**,** 8336–8346 (2011).

[19] Sepúlveda, B., Calle, A., Lechuga, L. M. and Armelles, G. Highly sensitive detection of biomolecules with the magneto-optic surface-plasmon-resonance sensor. *Opt. Lett.* 31**,** 1085–1087 (2006).

[20] Donolato, M. *et al.* On-chip manipulation of protein-coated magnetic beads via domain-wall conduits. *Adv. Mater.* 22**,** 2706–2710 (2010).

[21] Shoji, Y., Shirato, Y. and Mizumoto, T. Silicon Mach–Zehnder interferometer optical isolator having 8 nm bandwidth for over 20 dB isolation. *Jpn. J. Appl. Phys.* 53**,** 022202 (2014).

[22] Chetvertukhin, A. V. *et al.* Magneto-optical Kerr effect enhancement at the Woods anomaly in magnetoplasmonic crystals. *J. Magn. Magn. Mater.* 324**,** 3516–3518 (2012).
[23] Arregi, J. A., Riego, P. and Berger, A. What is the longitudinal magneto-optical Kerr effect? *J. Phys. D. Appl. Phys.* 50**,** 03LT01 (2017).
[24] Qiu, Z. Q. and Bader, S. D. Surface magneto-optic Kerr effect. *Rev. Sci. Instrum.* 71**,** 1243 (2000).
[25] Bader, S. D. SMOKE. *J. Magn. Magn. Mater.* 100**,** 440–454 (1991).
[26] Hunt, R. P. Contrast enhancement of the transverse Kerr effect. *J. Appl. Phys.* 38**,** 1215–1216 (1967).
[27] Girón-Sedas, J. A., Mejia-Salazar, J. R., Moncada-Villa, E. and Porras-Montenegro, N. Enhancement of the transverse magneto-optical Kerr effect via resonant tunneling in trilayers containing magneto-optical metals. *Appl. Phys. Lett.* 109**,** 1–5 (2016).
[28] Pohl, M. *et al.* Tuning of the transverse magneto-optical Kerr effect in magneto-plasmonic crystals. *New J. Phys.* 15**,** (2013).
[29] Allwood, D. A. *et al.* Over 40% transverse Kerr effect from Ni[sub 80]Fe[sub 20]. *Appl. Phys. Lett.* 92**,** 072503 (2008).
[30] Kleemann, W. Magnetooptical materials; Handbook of Magnetism; Wiley 2007. (2007).
[31] Berger, A., Pang, A. W. and Hopster, H. Magnetic reorientation transition of Gd(0001)/W(110) films. *Phys. Rev. B* 52**,** 1078–1089 (1995).
[32] Berger, A., Pang, A. W. and Hopster, H. Magnetic reorientation transition in epitaxial Gd-films. *J. Magn. Magn. Mater.* 137**,** 3–7 (1994).
[33] Florczak, J. M. and Dahlberg, E. D. Detecting two magnetization components by the magneto-optical Kerr effect. *J. Appl. Phys.* 67**,** 7520–7525 (1990).
[34] Dove, D. B. Photography of magnetic domains using the transverse Kerr effect. *J. Appl. Phys.* 34**,** 2067–2070 (1963).
[35] Oblak, E. *et al.* Ultrasensitive transverse magneto-optical Kerr effect measurements by means of effective polarization change detection. *J. Phys. D. Appl. Phys.* 50**,** 23LT01 (2017).
[36] Berger, A., Knappmann, S. and Oepen, H. P. Magneto-optical Kerr effect study of ac susceptibilities in ultrathin cobalt films. *Journal of Applied Physics* 75**,** 5598–5600 (1994).
[37] Berger, A. and Pufall, M. R. Study of generalized magneto-optical ellipsometry measurement reliability. *Appl. Phys. Lett.* 71**,** 965–967 (1997).
[38] Berger, A. and Pufall, M. R. Quantitative vector magnetometry using generalized magneto-optical ellipsometry. *J. Appl. Phys.* 85**,** 4583–4585 (1999).
[39] Arregi, J. A. *et al.* Study of generalized magneto-optical ellipsometry measurement reliability. *J. Appl. Phys.* 111**,** 1–8 (2012).
[40] Fowles, G. R. *Introduction to Modern Optics*. *Courier Corporation* (Dover Publications, New York, 1989).
[41] Idigoras, O., Palomares, U., Suszka, A. K., Fallarino, L. and Berger, A. Magnetic properties of room temperature grown epitaxial Co1− xRux-alloy films. *Appl. Phys. Lett.* 103**,** 102410 (2013).